Estuarine, Coastal and Shelf Science 264 (2022) 107700

Contents lists available at ScienceDirect

Estuarine, Coastal and Shelf Science

journal homepage: www.elsevier.com/locate/ecss

Seasonal variability of stratified flow properties in a Non-tidal Strait-A field study

Mehmet Ozturk *, Furkan Altas

Yildiz Technical University Civil Engineering Department Coastal and Harbor Laboratory, Turkey

ARTICLE INFO

Keywords:
Stratified flows
Exchange flows
Composite Froude number
The Bosphorus Strait
Non-tidal sea strait

ABSTRACT

The Bosporus Strait, connecting the Black Sea and the Marmara Sea in Turkey, is an example of a hydrodynamically complex strait. The Strait features a multi-layered (typically two-layer) flow system and is an example of (nearly) non-tidal exchange flow. A comprehensive measurement program including long- and short-term flow velocity, water level (near both entrances of the waterway), salinity, temperature, meteorological parameters (wind speed, wind direction, and atmospheric pressures at both entrances), and discharges of the Danube River were analyzed for the period between October 2004 and October 2005. The results show high variability in the layer velocities and salinities both temporally and spatially, and the typical two-layered current structure could be sustained for water level differences (the Black Sea minus the Marmara Sea) between zero and +45 cm. However, unidirectional flow, either northward or southward, is found at times, mostly in the fall and winter due to the severe meteorological (especially wind) conditions. The river inflow to the Black Sea is a strong control on the water level in the Bosphorus Strait—and, therefore, on the current structure—during the springtime and there is around a one-month phase lag between the peak river discharges and the peak water level increase in the strait. The relationship between the water level difference of the strait and the flow properties (thicknesses and flow rates) of both layers was also quantified from the cross-sectional current measurements. The velocity structures show both high qualitative and quantitative variability between the main channel and the side slopes of the cross-sections, and taking profile measurements on the slope without cross-sectional data may give a misleading assessment of the flow structure at the point of interest. There is strong mixing between the two layers throughout the strait causing a variation of 4–5 in the salinity of both layers between the two entrances. The non-dimensional flow rate calculation showed that the maximum exchange through the strait occurred for Composite Froude numbers (G^2) of around unity.

1. Introduction

Straits are linkages between two large water bodies, and often feature strong and stratified currents. There are around 30 major straits in the marginal seas of Europe alone, and a large number of these have characteristic topographical features (i.e., narrows or other complex geometric features) constraining the exchange of water. The flow structure and thickness of the layers vary through the strait due to the meteorological, morphological, and hydrodynamic conditions and the current properties show complex (highly nonlinear) behavior both temporarily and spatially. This complexity directly affects the circulation pattern in the strait. The interfacial shear, eddies, either near geometric irregularities or hydraulic adjustment, are the main reason for the mixing in the straits.

Like the Strait of Gibraltar, the Bosphorus Strait (Fig. 1a–c), which is part of the Turkish Straits System (TSS) along with the Dardanelles Strait, presents a classic example of exchange flows (Unluata et al., 1990; Besiktepe et al., 1993; Blain et al., 2009; Maderich and Konstantinov, 2002; Maderich et al., 2015). At Gibraltar, the exchange occurs between more dense (saline) Mediterranean water and Atlantic water through the Strait of Gibraltar (e.g., Armi and Farmer, 1988; Farmer and Armi, 1988). The flow variability at the Strait of Gibraltar is driven by the tide and atmospheric pressure (Lacombe and Richez, 1984; Candela et al., 1989; Harzallah, 2008). The Dardanelles and the Bosphorus Strait connect the Aegean Sea and the Black Sea via the Marmara Sea. Apart from the tidal dynamics, which are largely absent in the Bosphorus Strait, the flow there is very similar to that in the Strait of Gibraltar, in that they both feature a two-layered exchange system (Armi

* Corresponding author.,
E-mail addresses: meozturk@yildiz.edu.tr, meozturk@hotmail.com (M. Ozturk).

https://doi.org/10.1016/j.ecss.2021.107700
Received 14 September 2020; Received in revised form 2 December 2021; Accepted 7 December 2021
Available online 10 December 2021
0272-7714/© 2021 Published by Elsevier Ltd.

and Farmer, 1985; Bruno et al., 2013). The tidal amplitude is very low (O(10) cm) at both the Dardanelles and the Bosphorus Strait (Alpar and Yuce, 1998), and the water level difference ($\Delta\eta$) due to the intrusion of the freshwater excess into one of the adjoining seas (the Black Sea) and the meteorological set-up acting on the region, as well as the density differences ($\Delta\rho$) between the two ends of the strait, form the main controls on the exchange (Oğuz et al., 1990; Gregg and Özsoy, 2002; Maderich and Konstantinov, 2002). The Bab-el-Mandeb Strait, linking the Red Sea and the Arabian Sea (Murray and John, 1997) and the Great Belt between the Baltic and North Seas (Ottesen Hansen and Møller, 1990), are other significant examples of exchange flows.

A proper understanding of the flow dynamics of sea straits is crucial to waterway transportation, water quality, ecological concerns, and recreational events. To achieve this goal, it is necessary to have concurrent measurements of sufficient duration of velocity, water level, meteorology, water temperature and density both to quantify the general characteristics of the complex hydrodynamic behavior and to conduct a numerical model of the stratified flow properties of the waterway under consideration.

The Bosphorus Strait (Fig. 1) is a typical example of strait flow and is also one of the busiest international waterways in the world. The geographical conditions and navigational constraints of the Bosphorus make transit difficult for every kind of domestic and international vessel. The narrow channel, numerous course alterations, day-to-day changes in current, and bad weather conditions are additional parameters in the already risky navigation through the strait.

This paper describes the response of the stratified flow structure in a hydrodynamically complex sea -the Bosphorus Strait - to time-varying forcing on an annual scale. For this purpose, the concurrent velocity, water level and CTD measurements are described in the following section. These are shortcomings of the many field studies in the area so far, and were performed near the two entrances of the strait. In addition to quantifying the cross-sectional variability of the layered flow, an algorithm was also introduced to calculate non-dimensional layer properties (nondimensional discharges and thicknesses) as a function of the composite Froude number (G^2) to make the findings applicable to similar waterways. The remainder of the paper is structured as follows. The study area is described in Section 2. The details of the meteorological and hydrodynamics measurements performed in the strait are presented in Section 3. The variation in forcing mechanisms (i.e. meteorological, salinity difference and inflow conditions) acting on the Bosphorus Strait, and the response of stratified flow properties to them are analyzed in Section 4. The findings of the study are summarized in Section 5.

2. Study area

The Bosphorus Strait is 31 km in length, with a surface width varying from 0.7 to 3.5 km, averaging 1.3 km. The water depth along the main channel varies from 30 to 110 m. It has an irregular bottom profile with several major deep and sharp bends along its course. Two sills (Fig. 1b) play important roles in the strait's flow structure (Oğuz et al., 1990; Gregg and Özsoy, 2002). One of the sills is located at the northern entrance at a depth of 57–59 m, forming a natural extension of the strait into the Black Sea. The southern sill extends along the midchannel at a depth of approximately 28 m. Hereafter, the terms north and south refer to the Black Sea and the Sea of Marmara sides of the strait, respectively. The salinities of adjacent seas are quite stable and exchange takes place between the denser Sea of Marmara (salinity 38) and the Black Sea (18) throughout the strait. Due to mixing between layers, the salinity of the upper layer increases by around 5 from the north entrance to the south one, while decreasing by nearly the same amount in the opposite direction in the bottom layer.

The Bosphorus Strait generally presents a stratified two-layer current system, with the upper-layer current flowing southwards and the underlying flow towards the north. The two predominant controlling variables, which are density and water level differences ($\Delta\rho$ and $\Delta\eta$, respectively) between the adjacent seas, largely control the stratified structure (Özsoy et al., 1996; Ünlüata et al., 1990; Maderich and

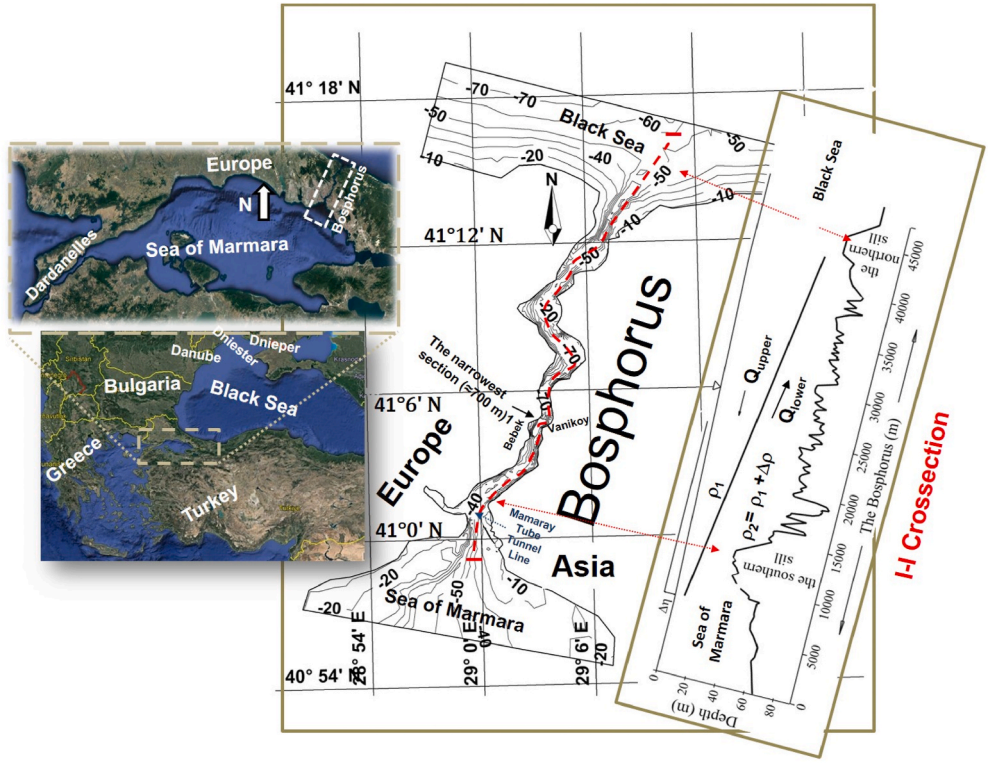


Fig. 1. Longitudinal view (right panel), schematic bathymetry (middle panel), schematic presentation of the two-layered flow structure (right panel) and the locator map of the Bosphorus Strait.

Konstantinov, 2002; Oguz, 2005; Kanarska and Maderich, 2008; Jarosz et al., 2011; Maderich et al., 2015; Gunduz et al., 2016; Yazıcıoğlu et al., 2016; Ozturk et al., 2017; Koşucu et al., 2019). In general, $\Delta\eta$ controls the upper layer flow while $\Delta\rho$ controls the lower layer flow.

The Black Sea is a nearly landlocked basin and hydrologically more dynamic than the Sea of Marmara, with a water level (η) generally higher than that in the Sea of Marmara (Fig. 1b). This water level difference drives a net southward flow through the Bosphorus Strait (Ünlüata et al., 1990; Sur et al., 1994; Stanev and Peneva, 2002). There are short- and long-term components of the water level difference ($\Delta\eta$). Wind set-up, atmospheric pressure, and the astronomical tide represent short-term forcing, and hydrological forcing (river discharges) is important at longer (seasonal) time scales. The long-term fluctuations occur at the seasonal scale (mostly from mid-spring to early-summer) and are more stable than those caused by short-term effects occurring at daily scales (Özsoy et al., 1996; Yuksel et al., 2008). The Danube River (Fig. 1c) discharges approximately 60% of the total river discharge into the Black Sea (Sur et al., 1994). The contribution of the Dnieper and Dniester Rivers (Fig. 1c) totals about one-third of the Danube discharge. The contribution of the remaining rivers is less than 20% of the total river runoff to the Black Sea. The period between April and October is relatively calm in terms of meteorological effects. For the remaining period of the year, however, severe meteorological conditions are more dominant and may cause extreme flow conditions in the strait; therefore, one-layer flow cases may develop in both directions depending on the wind structure (Yuksel et al., 2008). The thicknesses of both layers and their velocities show noticeable changes in time due to short-term changes in meteorological conditions.

The density difference between these two seas is the main mechanism for the northward lower layer flow (Fig. 1, right panel). Because the salinity variations of the adjacent seas show more stable (less fluctuating) behavior than the water level variations over the annual scale, the lower layer flow fluctuates less than that of the upper layer (Oguz et al., 1990). The salinity of the upper layer starts increasing from 17 to 18 from the entrance of the Black Sea and reaches around 20 to 25 at the entrance of the Sea of Marmara. The lower layer salinity, however, is around 40 at the southern entrance and around 35 at the northern entrance (Çolpan and Tugrul, 1995; Hubareva et al., 2008).

2.1. Previous studies on the Bosphorus Strait

One of the earliest studies on the hydrodynamics of the Bosphorus Strait was conducted by Çeçen et al. (1981). By making observations and visualizing the measured seasonal salinity and temperature profiles of the strait in 1980, they concluded that the lower layer flow did not always reach the Black Sea. Sumer and Bakioğlu (1981) studied the relationship between water level variation and stratified flow structure in the strait. Latif et al. (1991) showed that strong northern and southern winds would be able to block the flow in the opposite direction from time to time. The water level increase in the Black Sea could also block the lower layer flow of the Strait (Özsoy, 2000). Güler et al. (2006) carried out a detailed measurement program at various times between 2000 and 2003, measuring both short- and long-term current profiles at selected locations in the southern part of the Strait. They concluded that the mean current speed is around 0.8 m/s with peak velocities around 1.5 m/s in the southern part of the Strait during the relatively calm period of the year (May through September). They also showed that the meandering geometry of the Bosphorus Strait reversed flow in expanded areas. Jarosz et al. (2011) analyzed six-month-long Acoustic Doppler Current Profiler (ADCP) and Conductivity-Temperature-Density (CTD) data in the strait between September 2008 and February 2009 and showed that the upper layer discharges ranged from 12000 to 14000 m^3/s while the lower layer discharges ranged from 8000 to 10500 m^3/s. Doğan et al. (2001a and b) made instantaneous cross-sectional current measurements at each month at different locations in the Strait, while Altiok and Kayişoğlu (2015) did so only at the two entrances. Both studies estimated higher annual mean upper and lower layer discharges, however (13000 m^3/s for the upper layer and 7800 m^3/s for the lower layer) compared to the results of Jarosz (2011). Özsoy et al. (2016) showed that the layer's fluxes differed from north to south as upward entrainment fluxes from the lower layer to the upper layer increase the upper layer flow rate due to maximal exchange phenomena in the hydraulic control sections.

Previous field studies on the Bosphorus Strait, the main findings of which are summarized above (e.g., Güler et al., 2006; Yuksel et al., 2008; Altiok and Kayişoğlu, 2015), provide valuable contributions to our knowledge on the stratified flow structure in the strait. However, they (i.e., Güler et al., 2006) had either shorter measurement durations, or a lack of concurrent meteorological, water level and flow measurements, or lack of fluid (salinity-temperature-density) measurements (i.e., Yuksel et al., 2008; Altiok and Kayişoğlu, 2015) than the present study, preventing description of the proper relationship between the driving forces and the hydrodynamic structure in the strait. Therefore, the present study also contributes to filling the gaps in this regard.

3. Meteorological and hydrodynamic measurements in the Bosphorus Strait

The monitoring program was performed by the TAISEI Corporation, Japan, on behalf of the General Directorate of the Marmaray Project of the Ministry of Transportation, General Directorate of Ports, Airports and Railways Construction of Turkey (GDM). The measurement program, which focused mainly on the southern part of the strait, was aimed at monitoring the hydrodynamic structure of the Bosphorus Strait to reveal the characteristics of the stratified flow in the waterway, in order to determine the proper hydrodynamic conditions for the immersion process for each element of the Marmaray Tube Tunnel Crossing (Fig. 1), which is one of the biggest construction projects and the biggest single marine operation to date in Turkey. The current speed, wind, water level, atmospheric pressure, temperature, and salinity were measured at various locations in the Bosphorus Strait as part of this comprehensive environmental monitoring program. The list of measurement stations can be seen in Table 1 and Table 2, respectively. Because the salinity-temperature-density profiles were measured at locations very close to the current measurement stations, the same names were given to them as St. A, St. B, and St. C in Table 2. The locations of the long-term measurement stations are also shown in Fig. 2.

The current was measured by 600 kHz Aanderaa Recording Doppler Current Profiler (600 kHz-ADCP) devices. The measurement devices deployed on the bottom of the sea consisted of ADCP instruments, steel frames, and concrete blocks. The 600 kHz-ADCP took samples for 10 min with a 1-h sampling interval during the monitoring. A measurement cell size of 2 m was used with 2.5 cm/s and 1 cm/s accuracy in measuring horizontal and vertical velocities. The device has four beams and can measure velocities up to 5 m/s. The heading accuracy of the compass and tilting accuracy of the tilt sensor were $\pm 4^{\circ}$ and $\pm 1.5^{\circ}$. Maintenance of the devices was carried out at around one and a half months.

The water temperatures at the current measurement stations (St. A, St. B, and St. C) and the salinity at the sea bottom of St. B were measured by a temperature sensor and a conductivity sensor attached to the frame of the ADCP. The location of St. C was slightly changed a few times due to fishery-related problems. The yearly water temperature and salinity at the sea surface of St. D and St. E were measured by CTD sensors (Table 1).

A series of cross-sectional current measurements were also carried out along a transect (Sarayburnu-Üsküdar line in Fig. 2) near the southern end of the Strait to observe the stratification. Cross-sectional current distribution was measured by a 500 kHz-Acoustic Doppler Profiler (ADP) mounted on a ship. Bottom tracking was used as the vessel-velocity reference. The length of the measurement line was around ~1500 m and around 100 profiles were taken, which corresponded to ~15 m horizontal resolution. The blanking distance of the

Table 1
The durations and locations of the long-term measurements.

Stations	Periods		Characteristics	Measuring interval	Locations	Remarks
	Start	End				
St. A (d = 35 m) St. B (d = 26 m) St. C (variable, d ≈ 30 m)	October 01, 2004	September 30, 2005	Current speed (profiles), Current direction (profiles),Temperature (point), Salinity (point)	1 h	41°05′26.7′′N, 28°59′20.9′′E 41°0′52.4′′N, 28°59′53.6′′E 41°01′35.1′′N, 29°00′30.1′′E	Salinity (St. B), temperature (St. B and St. C) are point measurements at the bottom
St. D St. E	October 01, 2004	September 30, 2005	Water level (point), Temperature (point), Salinity (point)	1 h	41°01′31.4′′N, 29°00′30.3′′E 41°12′13′′N, 29°05′54′′E	Temperature and salinity (at St. D) are point measurements at the sea surface
St. F St. G	October 01, 2004	September 30, 2005	Wind speed (point), Wind direction (point), Air pressure (point)	10 min.	41°25′00′′N, 29°00′00′′E 41°00′00′′N, 29°00′00′′E	Calibrated forecast modeling data

Table 2
The time and locations of the Salility-Temperature-Density profiles.

Stations	Periods	Measurement Device	Locations
St. A St. B St. C St. H (d ≈ 60 m) St. I (d ≈ 70 m)	March 11 to March 13 (with 24-h interval), April 10, May 24, July 5, and August 23	CTD	~41°05′26.7′′N, ~28°59′20.9′′E ~41°0′52.4′′N, ~28°59′53.6′′E ~41°01′35.1′′N, ~29°00′30.1′′E 40°57′30.9′′N, 29°08′07.9′′E 41°13′44.3′′N, 29°08′07.9′′E

device and size of the beam cells were each 1 m. The ADP cross-sections were performed every 2 h during a storm for the first time in the Bosphorus Strait, from March 11 to March 13, and lasted 48 h. Additional single cross-sectional measurements were also carried out about every one and a half months in 2005. While making these one-time cross-sectional measurements, the corresponding salinity-temperature-density profiles close to the measurement line and at both entrances of the Bosphorus Strait were also measured (second column in Table 2 and Fig. 2).

4. Results and discussion

4.1. The meteorological setting

Either the whole of the Turkish Straits System (TSS) region or parts of it are impacted by the passage of cyclone systems, which usually last for 3–10 days, especially between May and September (Alpar and Yüce, 1998). Wind and atmospheric pressure variations, which occur due to these meteorological events, are short-term effects and cause notable water level increases at the two entrances of the Bosphorus Strait depending on the wind direction. In the case of increased net barometric

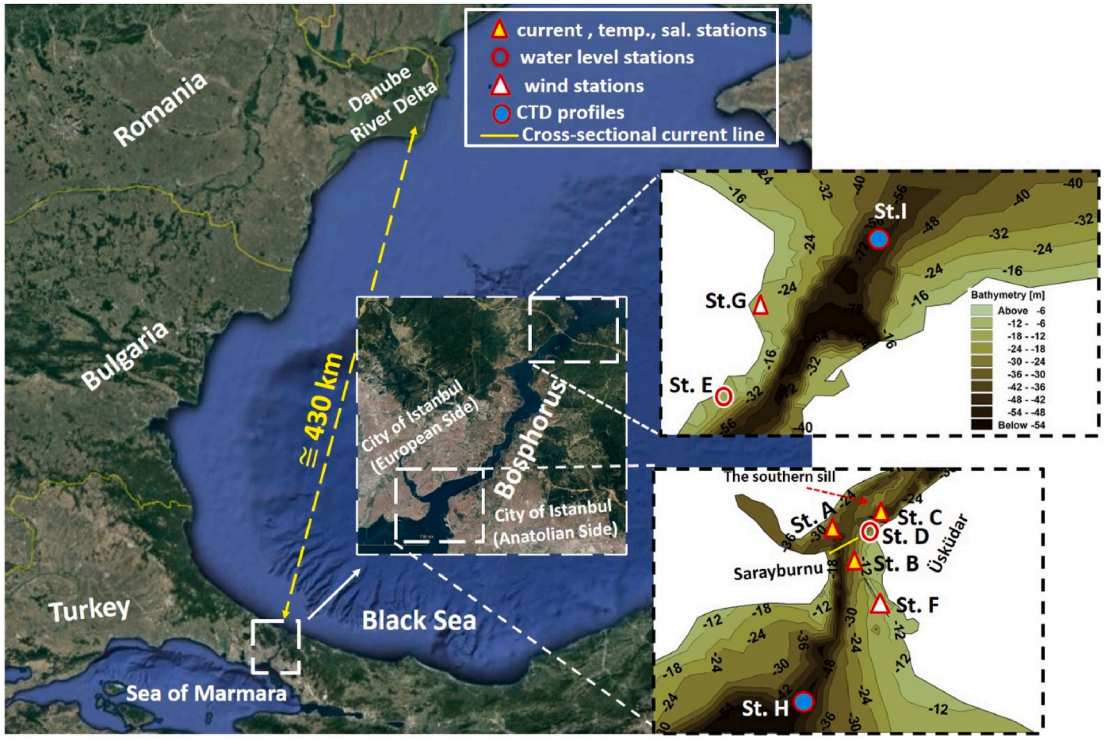


Fig. 2. The locations of measurement stations in the Bosphorus Strait.

flow due to strong and persistent northerly and southerly winds, the counter-flow to the wind becomes blocked and is pushed backwards (Ünlüata et al., 1990; Güler et al., 2006; Yuksel et al., 2008; Jarosz et al., 2011; Altiok and Kayişlioğlu, 2015).

Figs. 3 and 4 display winds and atmospheric pressures plotted using the meteorological measurements at the entrances of the strait. The annual wind climate of the strait was generally moderate for the period between October 2004 and October 2005 (Figs. 3 and 4a), classified as Calm (<~5 m/s) to Fresh Breeze (~10 m/s) on the Beaufort Scale. In the new data set, the prevailing wind directions are S-SW and N-NE at both entrances of the Bosphorus Strait (Figs. 3 and 4b), which is also comparable with the results obtained from the meteorological station around the strait (Deniz et al., 2013; Özdemir, 2018). However, the variation band of the wind direction is wider at the north entrance than at the south one. There were also occasional events in which the wind speeds were greater than 20 m/s, classified as Strong Gale (~20 m/s) to Storm (−25 m/s) and reaching ~ 25 m/s for the southerly wind. The atmospheric pressure patterns (Fig. 4c) followed very similar behavior to those of the wind speed (Fig. 4a) both south and north of the strait throughout the year. The correlations between St. F and St. G were higher for atmospheric pressures (the correlation coefficient is $R = 0.90$) compared to wind speeds ($R = 0.5$). The meteorological setup shows less variable behavior during the period from mid-April to October than for the rest of the observation period (Fig. 4a and c). However, some very pronounced storms (in late May, in July) occurred during this relatively stable period.

4.2. Hydrological setting: The effect of the in-flow conditions

Some previous studies such as Sur et al. (1994) and Yüksel et al. (2008) showed that the net freshwater flux into the Black Sea affected the long-term response of the mean sea level in the Bosphorus Strait. As explained before, the Danube supplies around 60% of the total freshwater runoff into the Black Sea (Global Runoff Data Centre (GRDC), 2007). Therefore, the Danube River discharge into the Black Sea is also the decisive mechanism in the water level behavior of the Bosphorus Strait, in addition to the meteorological setup. However, either they did not provide long-term measurements with a sufficiently high temporal resolution (such as the one-day resolution used here) or they did not have concurrent freshwater discharge, water levels and current measurements in the Bosphorus Strait which would have allowed detailed description of the relationship between these components.

Fig. 5a depicts the time history of water levels and the daily discharges of the Danube River for the observation period. A large seasonal variation was observed in the Danube River discharge ranging from 3590 to 14400 m^3/s (Fig. 5a and b). The most pronounced increase of around 9000 m^3/s occurred in two steps during the period between mid-February to mid-April (Case 1 from mid-February to early March and Case 2 from mid-March to mid-April as shown in Fig. 5b). At the end of this period, the peak discharges (≈14000 m^3/s) could be sustained for ~ 45 days. Due to the hydrological dominance and more stable meteorological set-up during the second half of the spring and the whole summer, the water level difference followed a less fluctuating pattern, averaging around $\Delta\eta = 0.40$ m, during this time (Fig. 5a).

Fig. 5b shows the variation of water level at the north entrance of the strait and the variation of daily discharge of the Danube River. To quantify the phase (time) lag between daily peak discharges of the Danube and the daily mean water level at the north entrance, two discharge increases were selected, Case 1 and Case 2 in Fig. 5b. The cross-correlation between these two parameters for these two cases indicates that the mean water level of the strait responds to the peak river discharges with around a one-month phase (time) lag (Fig. 5c). This phase lag may differ depending on the flow conditions in the year in question. In comparison, Sur et al. (1994) calculated a one-to two-month phase lag between this springtime freshwater intrusion into the Black Sea and the water level of the Bosphorus Strait.

4.3. Seasonal variations in the temperature and salinity of the layers

The surface salinity of the Bosphorus Strait fluctuates from around 15 to 25 throughout the observation period (Fig. 6a). More drastic salinity variations (around and greater than 5) occur during the fall and the winter than in the rest of the year. The surface salinity is nearly constant (≈17) from late May to July (Fig. 6a), following the peak Danube discharge intrusion into the Bosphorus during this period. The two other large variations in surface salinity, which last of the order of a week or more can be seen in mid-August and late September (Fig. 6b), respectively, following large Danube discharge fluctuations that occurred in July and August (Fig. 5a), respectively. The salinity of the bottom (≈38, St.B in Fig. 6b) is twice that of the top layer (St.D in Fig. 6a).

The variation range of surface water temperature is low compared to the salinity variation. Surface water temperatures follow a seasonal cooling-heating cycle and have lowest values in winter and highest values during late summer (Fig. 6a). Water temperatures near the two entrances of the strait (St.D and St.E in Fig. 6a) decreased from about 20 °C in October and reached a minimum value (~ 5 °C) in early February, then started increasing again, reaching 25 °C in September.

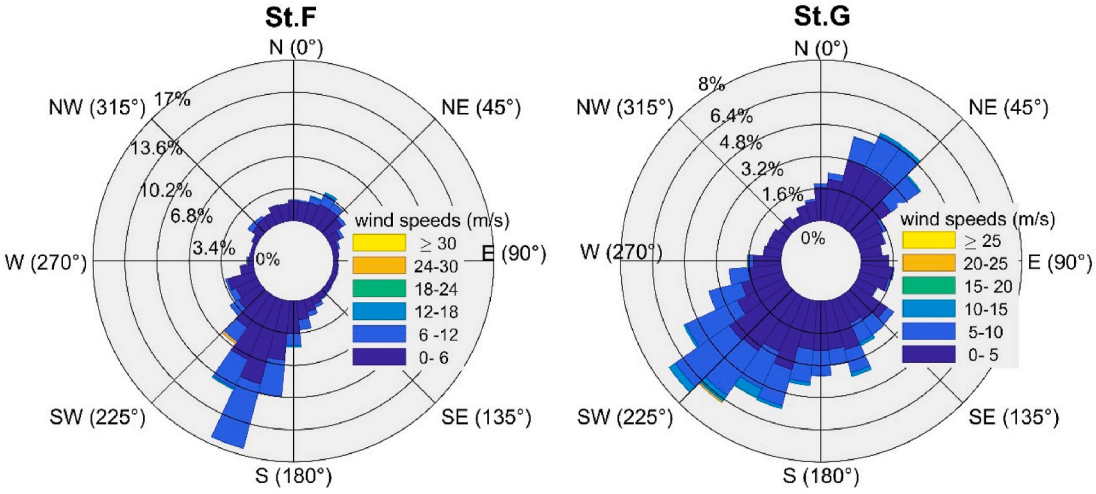


Fig. 3. The percentage of directional variation of wind speeds at St. F (south) and St. G (north) in the Bosphorus Strait for the annual scale (between October 2004 and October 2005).

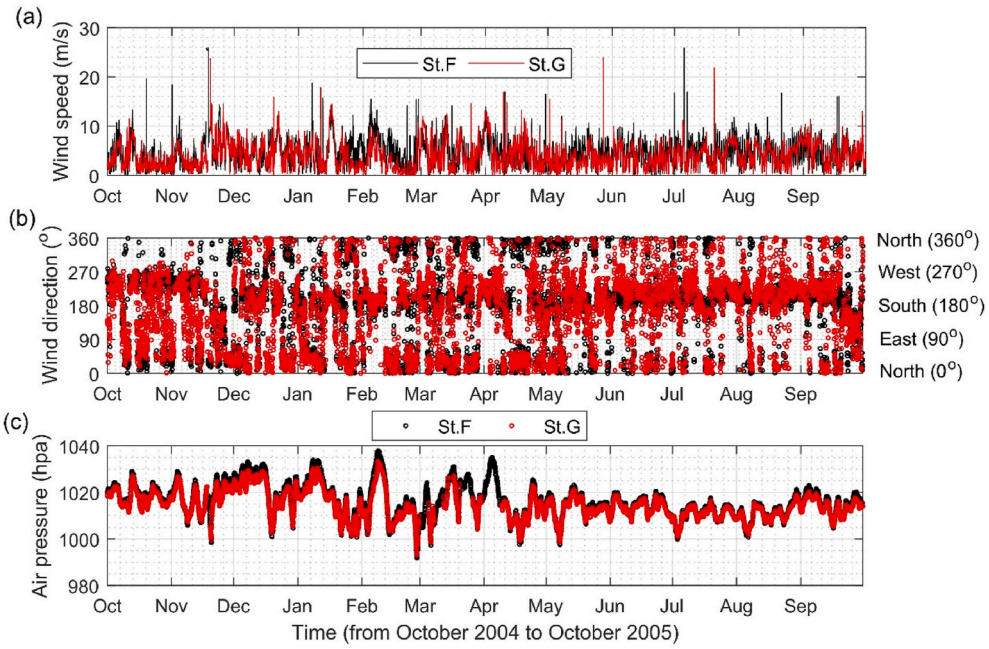


Fig. 4. The time history of wind speeds (a), wind directions (b), and atmospheric pressures (c) at St. F (south) and St. G (north) between October 2004 and October 2005.

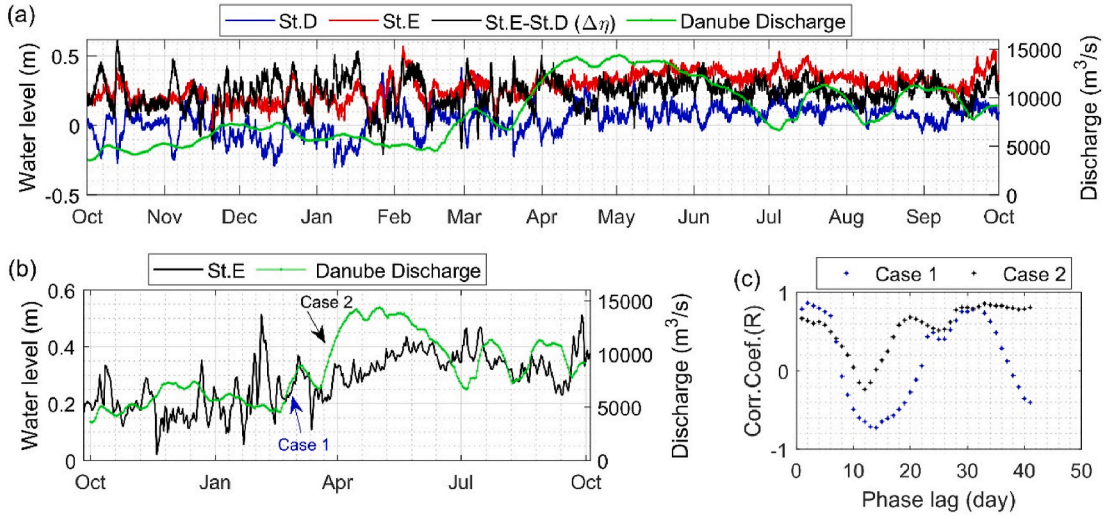


Fig. 5. The variation of (a) hourly water levels at St. D and St. E, the water level differences (Δηs) between St. E and St. D, and daily discharges of the Danube River (GRDC, 2007), (b) daily mean water levels at St. D and daily discharges of the Danube, (c) cross-correlation between the Danube discharges and mean water levels at St. E for two considered cases. Case 1 and Case 2 correspond to two discharge increases of the Danube River, which correspond to ≈4500 m^3/s from mid-February to early March and ≈8000 m^3/s between mid-March and mid-April in Fig. 5(b).

There was a notable seasonal variation in both temperature and salinity, and the effect of the meteorological set-up (Fig. 4a–c) and the discharge of the Danube on the salinity was very visible compared to the temperature (Fig. 6a). Due to the meteorological extremes (Fig. 4a–c), until mid-March the regular pattern of surface salinity was occasionally interrupted by fluctuations of around 5, lasting a few days.

The bottom temperatures and salinities of the water, generally dominated by dense Mediterranean water, are much more oscillatory compared to the surface (Fig. 6a and b). There are significant differences (>O (5 °C)) in temperature among closely located measurement stations (St. B and St. C in Fig. 2), which indicates the effect of the local topography (presence of the sill on the bottom) on the flow circulations/structures and thus on the fluid/flow properties. Both the seasonal variation range of the bottom temperature, which is ~4 °C at St. B and ~6 °C at St. C (Fig. 6band c) and salinities (~6–9 at St. B, Fig. 6b and c) is notably lower than the surface ones (~17 °C and 13 at St. D, Fig. 6a). In general, there was a tendency for an increase in bottom temperatures and salinities from mid-April to late December following the general decrease for the rest of the year (Fig. 6c). The salinities and temperatures of the surface increase from mid-February to early August then decrease (Fig. 6a and b), indicating a phase lag between salinity and temperature of the top and bottom of the strait.

4.4. Mixing and stratification

Salinity is a key tracer of the water masses in the Bosphorus Strait

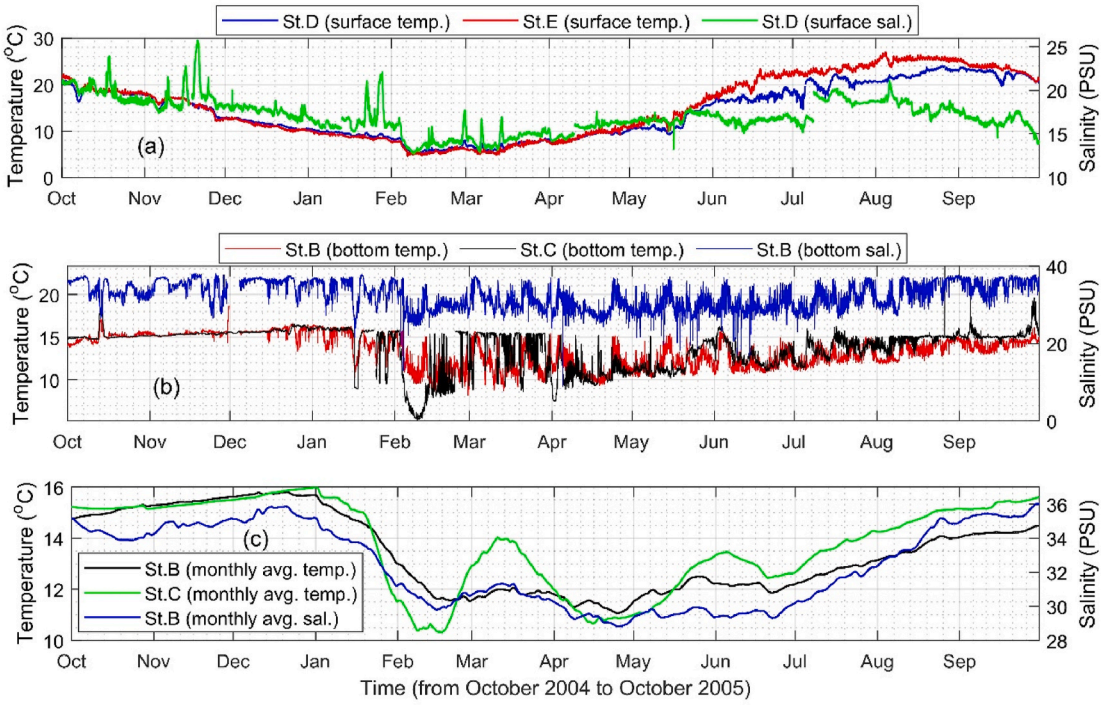


Fig. 6. The variation of (a) water surface temperatures, which are shortened as a *surface temp.* in the legend, at St. D and St. E and water surface salinity at St. D (shortened as *surface sal.* in the legend), (b) bottom temperatures at St. B and St. C (shortened as *bottom temp.* in the legend) and bottom salinity at St. B (shortened at *bottom sal.* in the legend), and (c) monthly moving average of (bottom) temperatures at St. B and St. C (labeled as *monthly avg. temp.*) and monthly moving average of (bottom) salinity at St. B.

and was observed via CTD measurements in 2005 during selected periods (Table 2). These data and concurrent cross-sectional current observations allow an estimation of brackish water inflow and the more saline (denser) water outflow along the considered cross-section.

Salinity, temperature and density observations with 24-h time resolution during a two-day-long southernly storm (from March 11th, 12 p.m. to March 13th, 12 p.m.), which caused a ~0.45 cm variation (decrease) in water level difference between both entrances, from the south and north of the strait are displayed in Fig. 7. Due to this mixing mechanism between the upper and lower layers throughout the strait, there is a salinity difference between the two entrances of the strait which is ≈ 22 at the southern entrance and ≈17 at the northern exit at the beginning of the storm (first column in Fig. 7). These results are compatible with previous studies (Yuksel et al., 2008; Oğuz et al., 1990). The thickness of the upper layer varies over time and is 18 m (~30% of the depth) on average at the Sea of Marmara entrance and around approximately 50 m at the north exit of the strait covering over 70% of the water column.

Mixing also causes a variation of around 5 in the average salinity of the bottom layer throughout the Bosphorus Strait at the beginning of the storm, which starts decreasing from 38 at the south entrance and reaches 33 at the north exit of the strait (Fig. 7e). The stratification is higher at the north entrance (Fig. 7e), while mixing is stronger at the south entrance (Fig. 7a) at the beginning of the storm. At the end of the storm, however, due to the resistance of the southward upper layer flow to the strong wind-induced water level increase that contributes to forcing the balance in favor of the northward lower layer, stratification decreases to the north. The thickness of the mixed layer close to the north entrance increased from a few meters at half the duration to around 25 m at the end of 48 h (Fig. 7e). The strongest mixing is observed close to the southern sill region of the strait (Fig. 7b-c-d), especially at St.B which is located to the south of the sill.

The salinity, temperature, and density profiles at various times in the Bosphorus Strait are plotted in Fig. 8. In general, stratification is much stronger close to the southern exit than at the northern exit at all considered instances (Fig. 8b-c-d) while mixing shows the opposite behavior. Similar to the storm conditions (Fig. 7b-c-d) the mixing-stratification pattern shows different behavior at closely located sites (St. A than at St. B and St. C in Fig. 8) denoting the significance of complicated geometrical features (i.e. sharp bending and the sill on the bottom) on the local hydrodynamic behavior in the strait.

4.5. Flow structure

4.5.1. Long time variability of flow profiles

Fig. 9 displays time series of current profiles recorded at the southern Bosphorus Strait (St. A, St. B, and St. C in Fig. 2). The minus and plus velocities indicate the southward and northward along-channel velocities, respectively. At all three locations, the observations mostly show a two-layer structure of the exchange flow in the strait. The percentage and magnitudes of the current speeds show also significant temporal and spatial variations, which are similar to the salinity-temperature –density profiles, at these nearby locations. The local geometric features of the main channel cause this variability in flow behaviors. For example, the main channel is oriented to the Northeast-Southwest (NE-SW) at St. A, North-South (N–S) at St. B, and East-South-East (ESE) to West-South-West (WSW) at St. C. In addition to this, local geometrical variations such as an expansion in channel width or the presence of a headland at Saryburnu (Figs. 1 and 2) affect the magnitudes of the velocities by causing a local circulation pattern moving opposite (from Sarayburnu to the north) to the main flow direction in the south (Güler et al., 2006; Öztürk et al., 2012). This flow pattern probably affects the current structure at St. A (Fig. 9a). The current velocities are the smallest and show much more complicated behavior over the vertical at St. A compared to the other stations (Fig. 9a-b-c). The typical two-layer flow structure, however, is much more visible at St. A (Fig. 9a) and St. B (Fig. 9b) compared to St. C (Fig. 9c). The largest velocities are observed at St.B because it is further away from the southern sill than St.A and St.

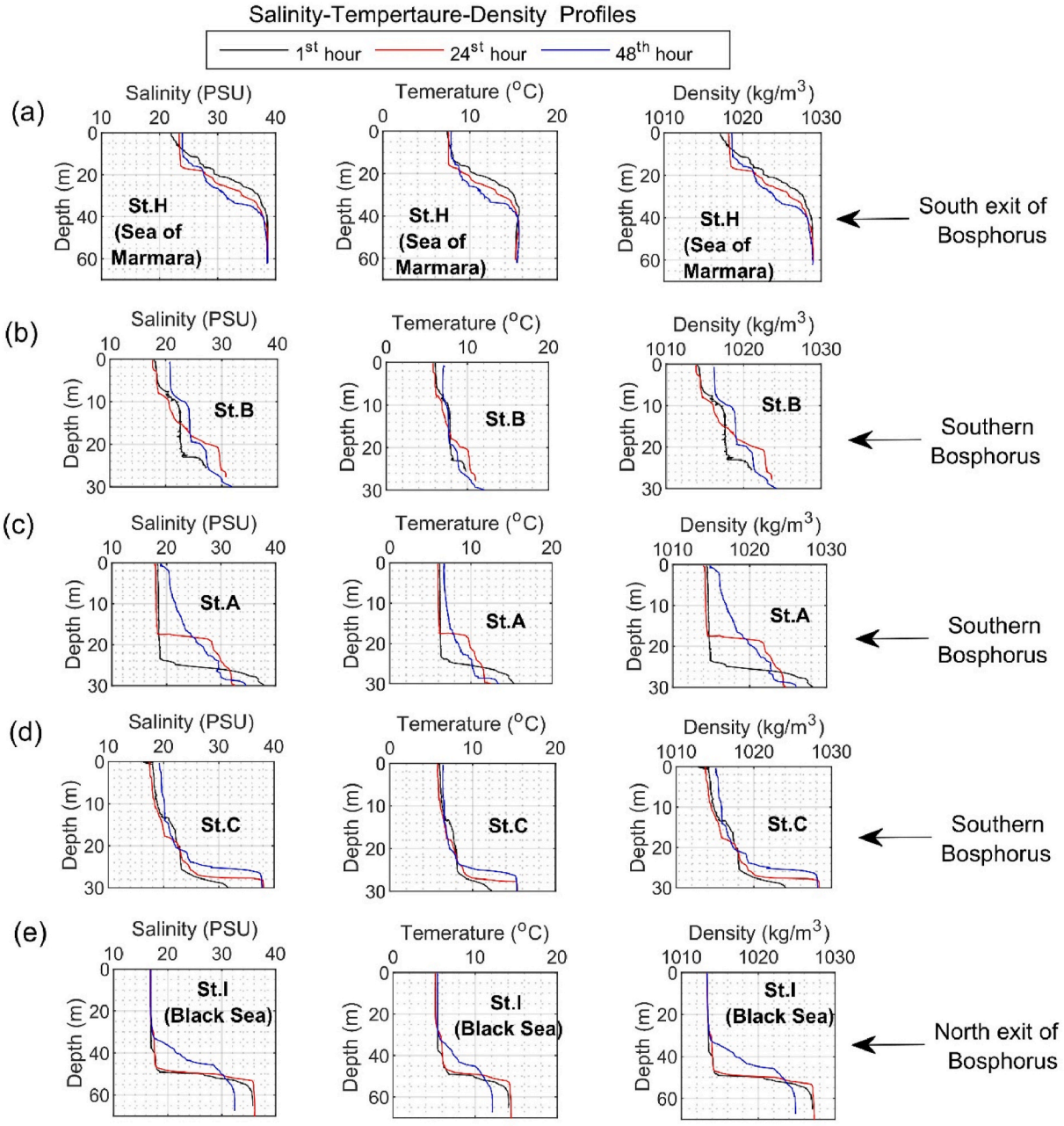


Fig. 7. The variation of salinity, temperature, and density profiles at St. H (a), St. B (b), St. A (c), St. C (d), and St. I (e). Profiles were obtained from CTD measurements between March 11th, 12 p.m. and 13th, 12 p.m. every 24 h.

C (Fig. 2). The last two measurement stations are located on each side of the sill, which show more dominance in their flow structure than St. B.

The peak current velocities, which have maxima around 2.5 m/s at St. B, were reached for one-layer flow cases due to northern storm events (e.g., mid-January, early February, and early April in Fig. 9a-b-c), which mostly occurred during the fall and winter. Those single layer southward flow velocities were generally measured for $\Delta\eta$>0.40 m water level difference conditions (Fig. 5a). However, it should be noted that the two-layered flow structure could survive in the strait even though $\Delta\eta$ > 0.40 depending on the duration of the water level increase. Öztürk (2013) showed that for a longer duration of the same water level difference between the two entrances, for example, the lower layer could resist the momentum of the upper layer water mass and survive in the strait.

The one-layer flow conditions in the opposite direction (northward) are evident for negative and around zero water level differences between the two entrances of the Bosphorus Strait, which indicates the higher water level of the Sea of Marmara than of the Black Sea. Peak northward current speeds of the order of 1 m/s (Fig. 9b and c) were observed at St. B during the southern storms in the late autumn or winter (i.e., late November, late January, and late February) for $\Delta\eta$~-0.20 m (Fig. 5a). The typical two-layer flow structure of the Bosphorus Strait (Fig. 9a-b-c) is more visible and stable during the (meteorologically) calm period (between May and October) of the year (Fig. 4a–c and 5a).

Readers should also bear in mind that none of the three measurement stations above is located on the main channel (not on the thalweg (deepest) points of their cross-sections). Therefore, the current structures are specific to these points rather than reflecting the general behavior of the cross-sections. As shown in the following section, the cross-sectional flow measurements show that different flow structures

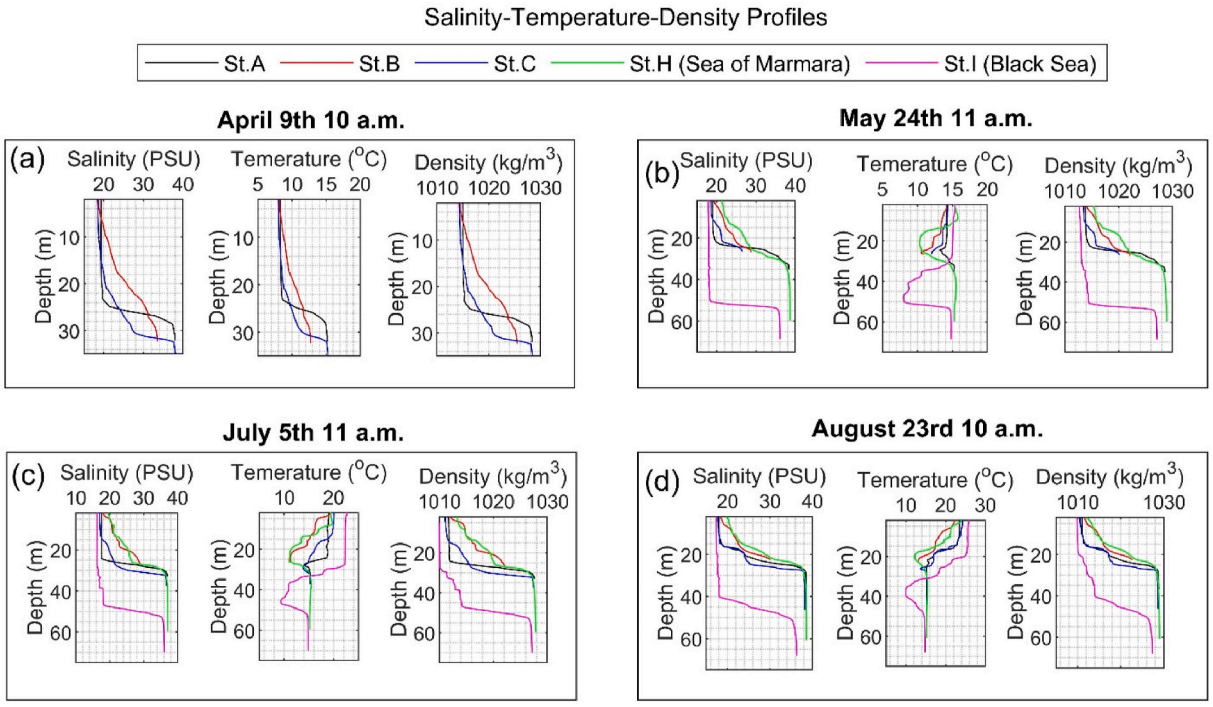


Fig. 8. The Salinity, temperature and density profiles close to both entrances and at the southern part of the Bosphorus Strait on April 9th, 10 a.m. (a), May 24th, 11 a.m. (b), July 5th, 11 a.m. (c), and August 23rd 10:00 in 2005 (d). The measurements were not available on April 9th 10:00 at St. H (the Sea of Marmara) and St. I (The Black Sea).

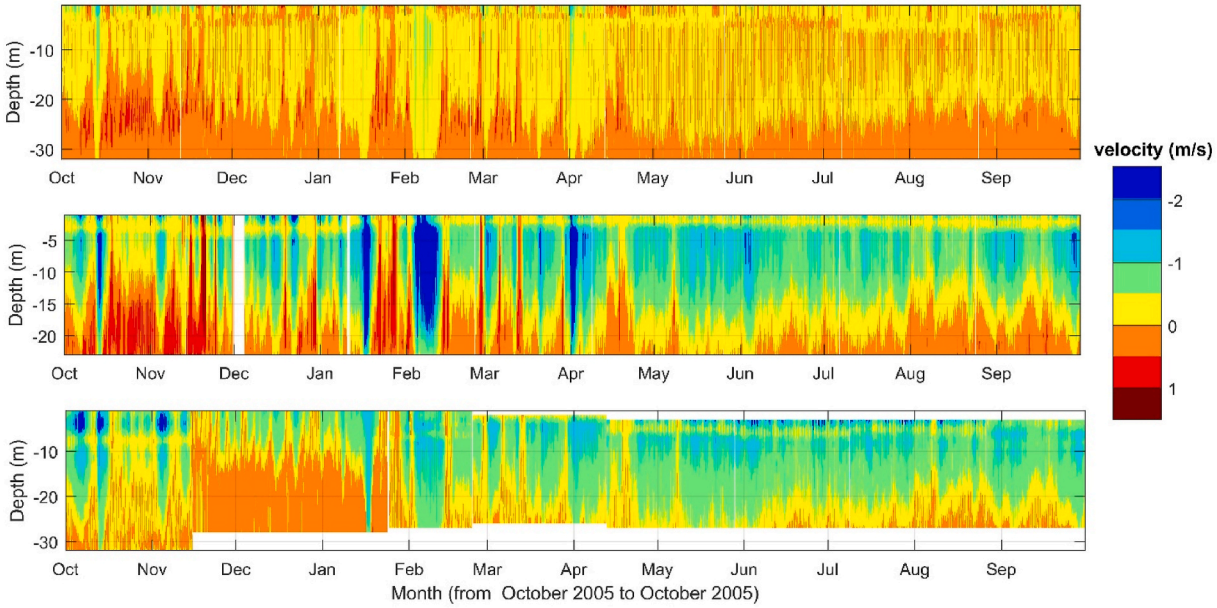


Fig. 9. The variation of current profile at St. A (a), current profile at St. B (b), and current profile at St. C (c). The white vertical strip in Fig. 9bd denote no measurement during this period and the location of St. C was changed a few times due to fishery problems.

may develop between the main channel and the side slopes (i.e., two-layer flow around the main channel and one layer flow on the slopes).

4.5.2. Crossectional variability of flow

Cross-sectional current measurements were performed along an approximate line close to the southern exit of the strait between Sarayburnu and Üsküdar (Fig. 10a) in 2005 during selected periods: from March 11th at 12 p.m. to March 13th at 12 p.m., on April 9th at 10 a.m., on May 24th at 11 a.m., on July 5th at 11 a.m., and on August 23rd at 10 a.m. The measurements were applied with 1 m vertical resolution at about 15–20 m horizontal resolutions.

The first set of cross-sectional measurements was continuous and applied every 2 h throughout the 48 h between noon on March 11 and noon on March 13. A decrease of ~10 hPa (hPa) occurred in atmospheric pressure (Fig. 11a) during this period, and the wind direction shifted to the north after blowing in the south for about 12 h (Fig. 11b). This meteorological setup causes a ~0.45 m variation (decrease) in water level difference between the two entrances of the strait (Fig. 11a).

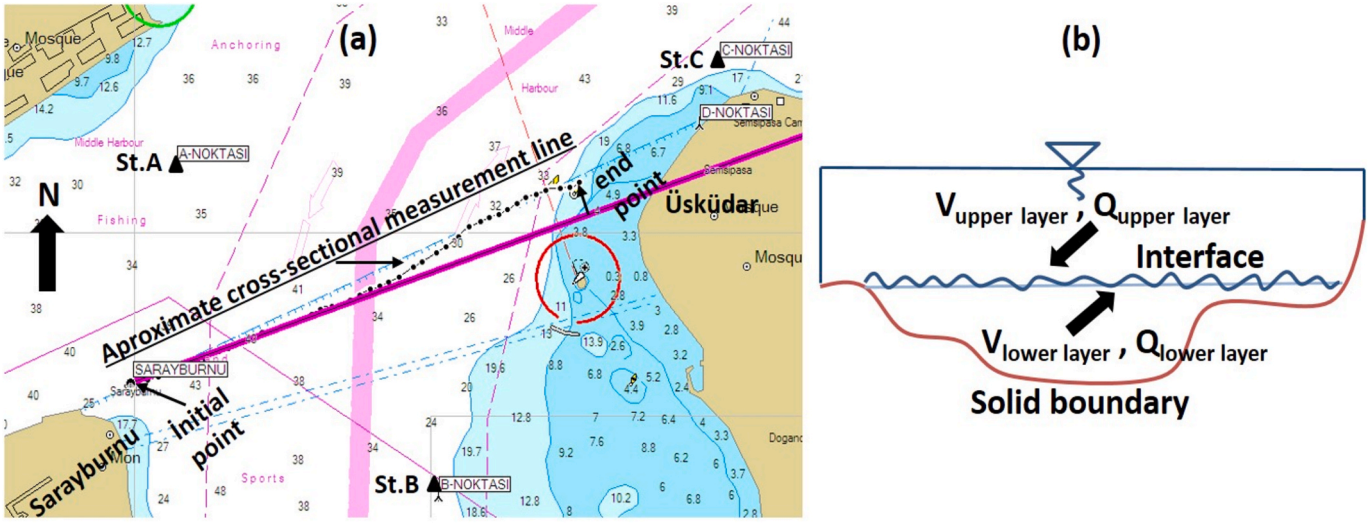


Fig. 10. (a) The approximate location of the cross-sectional measurement line between Sarayburnu on the west and Üsküdar on the east (Fig. 2), (b) the schematic presentation of the cross-section and principal characteristics of the layers.

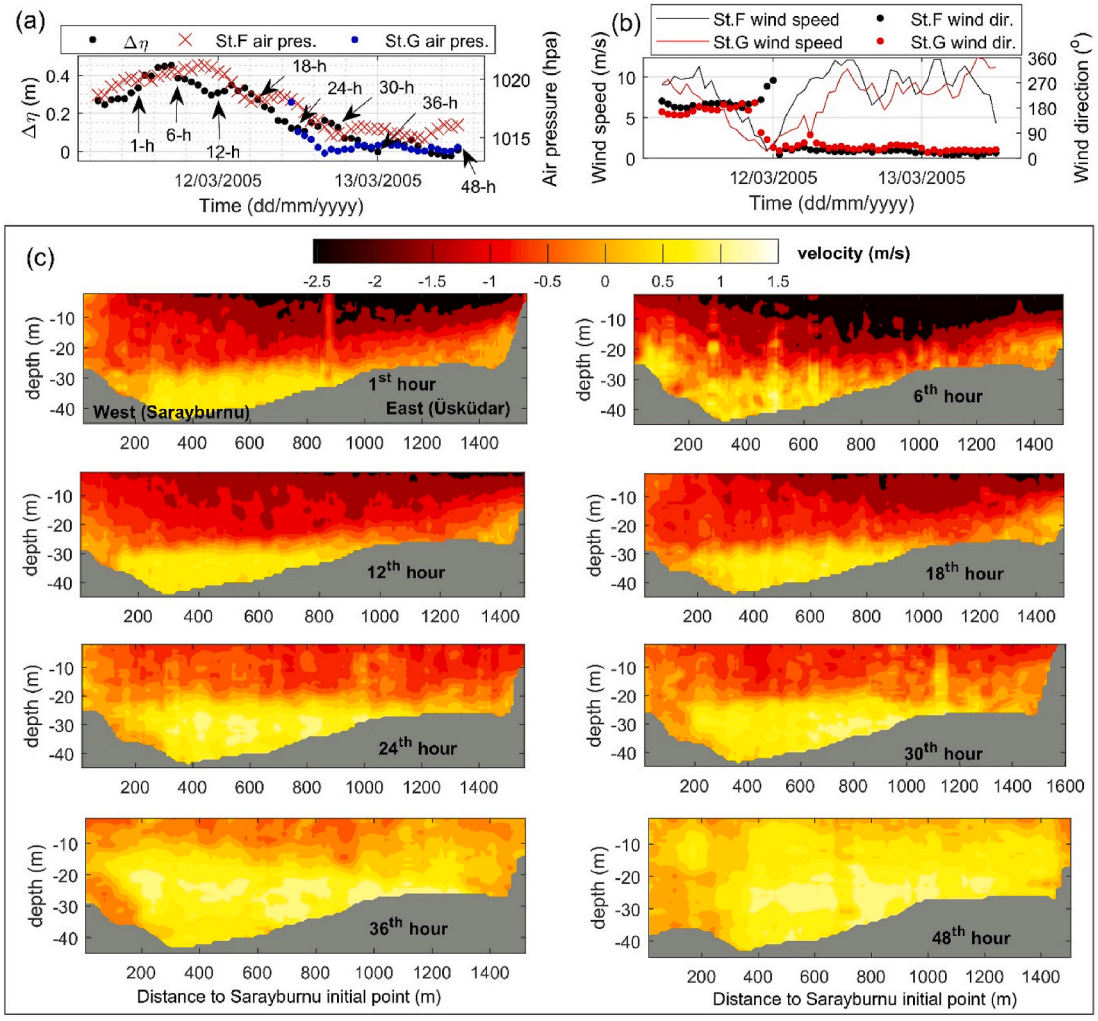


Fig. 11. The time history of water level difference (Δη) of the Bosphorus Strait and atmospheric pressure (a), wind properties (b), and cross-sectional current velocities at every 6 h (c) due to the meteorological set-up acting on the Bosphorus Strait between March 11th, 12 p.m. and March 13th, 12 p.m. in 2005.

The cross-sectional current field responds quickly to the water level variation difference and the typical two-layer flow structure of the strait at the beginning of the measurement, which corresponds to $\Delta\eta = 0.35$ m (1-h in Fig. 11a), gradually weakens and disappears after 48 h (Fig. 11c). The peak velocities of the upper and lower layers are around 2 m/s in the south at the top and 1.5 m/s in the north at the bottom. Due to the resistance of the upper layer flux to the lower one, several instabilities are observed in the velocity isoline after the 24th hour of the storm (the last four panels in Fig. 11c).

The magnitude of the flow velocity is approximately of the same order between the slopes of the cross-section line (Fig. 11c) and three closely located velocity measurement stations (Fig. 12). The velocities on the main channel of the cross-section line, however, are much stronger compared with those at St. A, St. B, and St. C. As mentioned above, none of these monitoring stations were deployed in the main channel (Fig. 10a), and therefore one layer northward flow dominates the water column (Fig. 12) earlier than it does in the main channel section (Fig. 11c). Considering the 6th-, 12th-, and 18th-hour current structure in Fig. 11c, for example, the flow is one layer at most of the right slope and at the left end of the cross-section while it presents a two-layer flow at the main channel. This shows the importance of selecting measurement locations as close to the main channel as possible to gain more convenient data for evaluating the physical properties of stratification for this kind of waterway.

Fig. 13 displays cross-sectional current measurements between Sarayburnu-Üsküdar and flow profile measurements corresponding to those various times in 2005. The 100 h-long variations of water level difference between the entrances of the strait covering each cross-sectional measurement are also given in Fig. 14. As seen from Fig. 14 (right panel), the time gradient of the water level decrease ($\Delta\eta/T$) is larger in April during those 100-h periods compared to the remaining cases. Due to the dominance of the Danube River discharges on the water level of the strait, the slope is mildest in the May case.

The cross-sectional and single-point (profile) velocity measurements show significant variation in behavior. The cross-sectional flow structures resemble the characteristic two-layer flow pattern for all considered cases (Fig. 13a–d left panels). However, there is one layer flow in the south at St. B and St. C and mostly one layer or no-flow at St. A (Fig. 13a–d right panels). The response of the cross-sectional current structure to the water level shows a temporary difference, which is especially notable in August 2005 (Fig. 13d). As the much more stable freshwater inflow from the major rivers dominated the water level difference during the late spring and early summer, the velocity isolines of the cross-sectional current are much smoother in the first three cases (the fifth panel in Fig. 13a-b-c) than the last one (the fifth panel in Fig. 14d). The temporal variation of water level difference is most stable in May (Fig. 14), as the river inflow reached its peak during this time (Fig. 5a).

4.6. Volume fluxes of the layers

The volume fluxes of both layers in this study are calculated as follows:

$$Q_i = \sum_{j=1}^{n}\sum_{k=1}^{m} V_j \cdot (\Delta x)_j \cdot (\Delta z)_k;\ \Delta x_{j,k} = 0.5 \cdot \left(x_{j-1,k} + x_{j+1,k}\right);\ \Delta z_{j,k} = 0.5 \cdot \left(z_{j,k-1} + z_{j,k+1}\right) \quad (1)$$

where i = 1,2 corresponds to the upper and lower layers, respectively; j = 1, …,n is the number of measurement profiles from the initial point (west, Sarayburnu) in Fig. 7a and k = 1, …., m is the number of points in the profiles; V_j is the velocity component acting perpendicular to the center of the $\Delta x \cdot \Delta z$ area; Δx is the alongside distance on the line in Fig. 10b; and Δz is the vertical distance on the considered profiles, which is constant and equal to 1 m. The volume fluxes and thickness of the layers on each profile were determined by the direction of current velocities. The southern directions were considered as the indicator of the upper layer flow, while the northern directions were the counter-flowing layer.

There is a strong linear relationship between water level difference ($\Delta\eta$) and the flow rates of the layers in the Bosphorus Strait (Fig. 15a and c). Because water level difference is the main driving force for the upper layer, the correlation is higher for the upper layer flow than for that of the lower one. The correlations between $\Delta\eta$ and thickness of the layers at thalweg (the deepest) points are nearly the same for both layers (Fig. 15b and d). $\Delta\eta \approx 0.15$ m corresponds to the equilibrium state for the layer discharges in the Bosphorus Strait, which are around 20,000 m^3/s (Fig. 15a and c). For around $\Delta\eta < 0$ m and $\Delta\eta > 0.45$ m, the two-layer flow shifts to one layer flow, which is in the south at the former case and in the opposite direction at the latter one, at the cross-section line close to the southern exit. Some earlier studies also reported a similar variation of the volume fluxes (Doğan et al., 2001a and b; Altiok and Kayişoğlu, 2015) by making cross-sectional measurements at different locations of the Bosphorus Strait. Altiok and Kayişoğlu (2015) analyzed the monthly variation of the layer discharges over the long term (between January 1999 and January 2010) while Doğan et al.

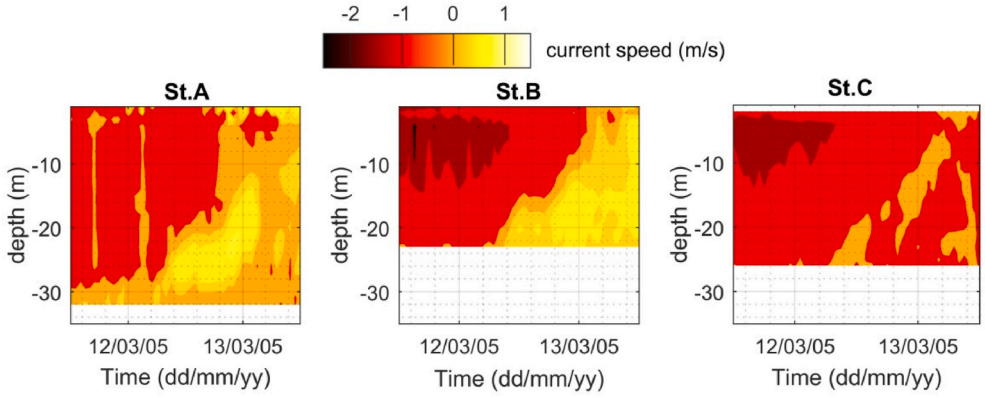


Fig. 12. The current velocity profiles at southern Bosphorus Strait (at St. A, St. B, and St. C) during the storm between March 11 12:00 and March 13 12:00.

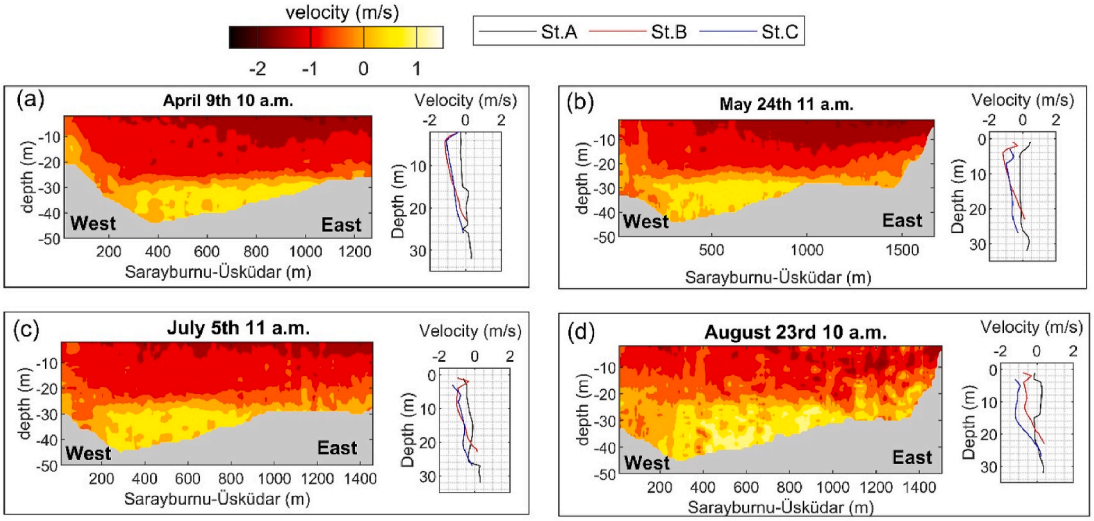


Fig. 13. The snapshots of cross-sectional current velocity distribution between Sarayburnu (west) and Üsküdar (east) lines and velocity profiles at the southern part of the Bosphorus Strait on April 9th at 10 a.m. (a), May 24th at 11 a.m. (b), July 5th at 11 a.m. (c), and August 23rd at 10 a.m. in 2005.

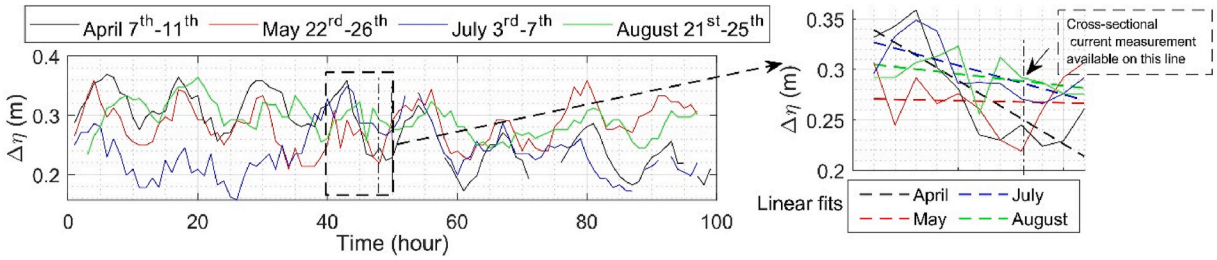


Fig. 14. The time history of water level difference (Δη) of the Bosphorus Strait for 100-h duration covering the cross-sectional measurement moments in Fig. 13a-b-c-d.

(2001a and b) did the same over the short term (July, August, and September). The discharges of the layers are comparable—especially in Altiok and Kayişoğlu (2015) study—to the result of the present study (Fig. 15a and c). However, the corresponding water level difference between the two ends of the strait to the discharges is unknown in all of these studies, which makes it difficult to obtain a convenient comparison between the previous findings and the present ones.

The volume flux results in the present study were also non-dimensionalized to increase the applicability of the present study's findings to similar waterways. For this purpose, Composite Froude number (G^2) and non-dimensional unit flow rates (q*) of the layers and non-dimensional unit layer thicknesses (h*s) were used.

G^2 is the most widely used non-dimensional parameter for free surface stratified flows and given by (2) (Armi, 1986):

$$G^2 = F_1^2 + F_2^2 + (1-\gamma)F_1^2F_2^2 \tag{2}$$

where $i = 1$ and 2 represents the upper and the lower layer, respectively, $F_i^2 = u_i^2/g'h_i$ are the Froude numbers of each layer and h_i is the mean thickness of each layer and calculated as A_i/B_i, where A is the area of each layer and B is the surface width of the upper layer and the width of the interface for the lower one. In Eq. (1), $g' = (1-\gamma)g$ is the reduced gravitational acceleration, $\gamma = \rho_1/\rho_2$, and ρ_1 and ρ_2 is the density of the upper and lower layers. For small non-dimensional density differences $(1-\gamma) \ll 1$–like in the present study–Eq. (2) can be simplified as $G^2 = F_1^2 + F_2^2$.

q*s and h*s for each layer was calculated by (3) as follows:

$$q^* = \frac{q_i}{\sqrt{gh_m^3}},\ h^* = \frac{h_{i,thalweg}}{h_i} \tag{3}$$

where $q_i = Q_i/B_i$ is the unit flow rate of each layer, Q is the flow rate of each layer, g is the gravitational acceleration, and $h_{i,thalweg}$ is the water depth at the thalweg.

The relationship between q*, h* and G^2 is given in Fig. 16. In two-layer flows, similar to single-layer flows, $G^2 = 1$ corresponds to the critical flow conditions, and one of the layers vanishes during this case (Armi, 1986). This phenomenon takes place at so-called "control zones", or "control sections" in a strait. The "maximal exchange" occurs at these locations. The control sections are generally located at topographical features in a strait such as the crest of sills and the narrowest section of contractions (Armi and Farmer, 1986). There are three control sections in the Bosphorus Strait (Oguz et al., 1990): the northern sill, the southern sill, and the narrowest section (Fig. 1). The cross-sectional measurement line in the present study (Fig. 2 bottom right panel and Fig. 10a) was quite close to the southern sill. $G^2 < 1$ and >1 correspond to subcritical and supercritical flow conditions, respectively.

The flow was mostly subcritical close to the southern sill (Fig. 16a-b-c-d). Similar to Fig. 15a and c, the strength of the linear relationship between G^2 and non-dimensional q* is notably higher for the upper layer than for the lower one. Incompatible with the hydraulics of two-layer flow, the maximum exchanges were reached for G^2 at and around 1, which corresponded $\approx q^*_{total} = q^*_{upper} + q^*_{lower} \cong 0.06$ (Fig. 16a and b) and $h^*_{total} = h^*_{upper} + h^*_{lower} \cong 1.30$. Those non-dimensional parameters correspond to a total discharge of ≈55,000 to 60,000 m^3/s and Δηs of ≈0.40–0.45 m in the Bosphorus Strait.

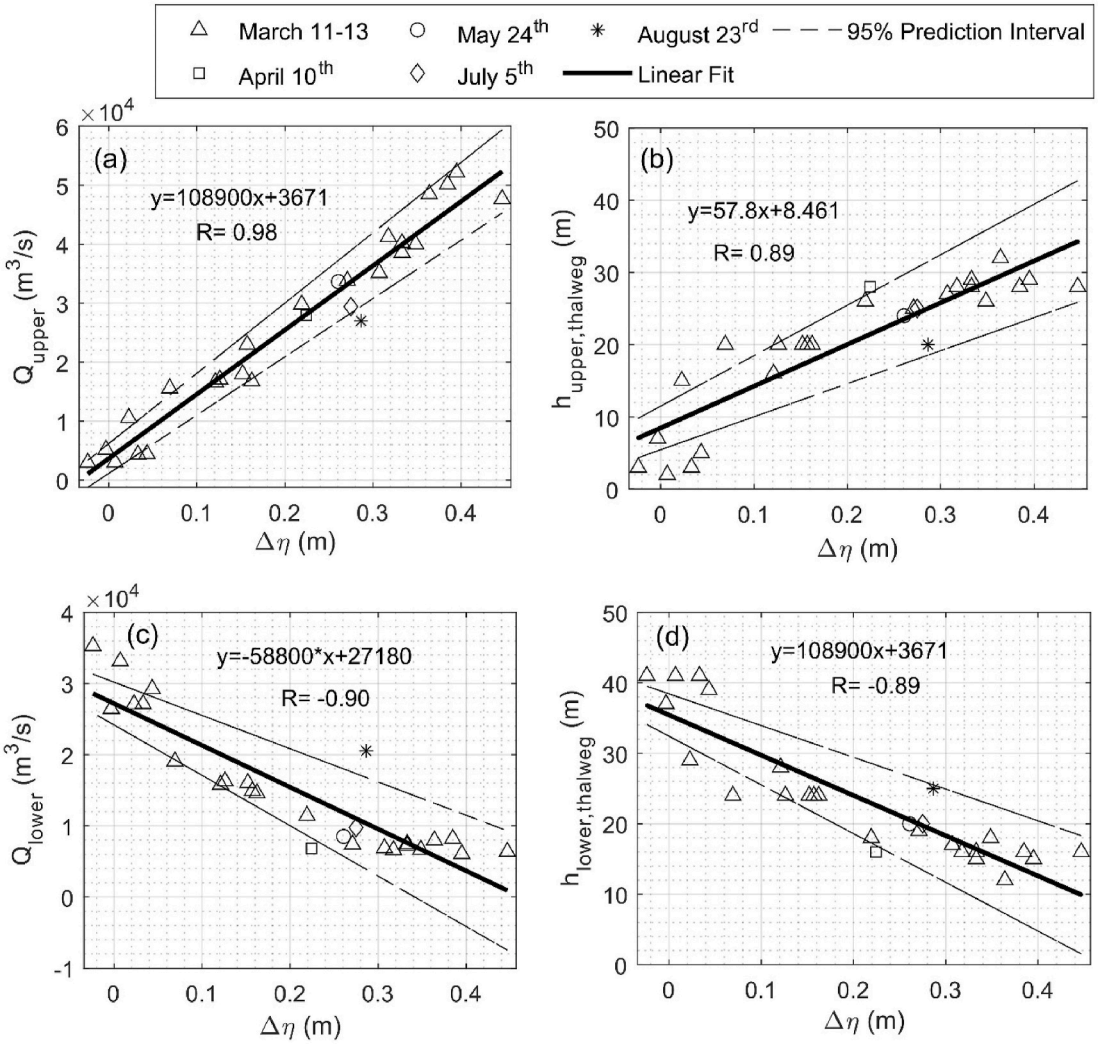


Fig. 15. The relationship between water level difference (Δη) of the Bosphorus Strait and layer properties (volume fluxes and thicknesses). The volume fluxes were calculated using twenty-eight cross-sectional velocity measurements: twenty-four cross-sectional current measurements between March 11 and 13 with a 2-h interval, and four instantaneous measurements with around and half-month intervals at various times (on April 9, May 24, July 5, and August 10) in 2005 between Sarayburnu (on the west) and Üsküdar (on the east) close to the southern exit of the strait.

5. Summary and conclusions

The flow structure of a sea strait, which is a link between two distinct water bodies (e.g., the Black Sea and the Mediterranean), is generally stratified and could show complex spatiotemporal variations depending on the driving conditions (meteorological, morphological, and hydrodynamic) acting on its boundaries. This complexity directly affects the stratified flow structure and water exchange throughout straits, which has significant importance in many aspects, such as transportation, migration of fish species, and recreational events.

In the present study, the response of the hydrodynamic structure of a non-tidal strait (Bosphorus Strait) to its driving forcing conditions was evaluated in light of the findings of a detailed measurement program, which was made between October 2004 and October 2005. In the long-term measurement program, the annual current profiles at three selected locations at the southern part of the strait, the water level measurements close to both entrances of the waterway, the surface salinity and temperature at water level measurement locations, and the bottom salinity and temperature measurements at current measurement locations were performed. The annual variation of the meteorological setup was also analyzed using the findings at stations located in both the north and the south of the Bosphorus Strait. Additionally, short-term cross-sectional current measurements along the line, which was very close to the bottom sill, at the southern part of the waterway, and the corresponding salinity-temperature-density measurements both close to the cross-sectional line and close to both entrances of the Bosphorus Strait were utilized. The highlights of the present study may be given below —and with the sketch diagram in Fig. 17— as follows:

- The water level difference (Δη) between the two entrances of the Bosphorus Strait, which is the driving force for the southward upper layer flow, showed notable fluctuations with a maximum of around 80 cm over the annual scale. The meteorological set-up (wind speed and atmospheric pressure) is much more severe and decisive over Δη during the autumn and winter of the year (Fig. 4), which has a duration of a few days causing large water level fluctuations (O(>40 cm)) (Fig. 5a). During this period, the typical two-layer flow structure of the strait frequently disappears and one layer, either southward or in the opposite direction depending on the wind direction, dominates the water column at the measurement locations (Fig. 9a-b-c, 11c, 12). The freshwater intrusion to the Black Sea from the major rivers (especially the Danube River) reaches the Bosphorus Strait with around a one-month phase (time) lag (Fig. 5c) and controls the water level difference (Fig. 5a) and, thus, the current

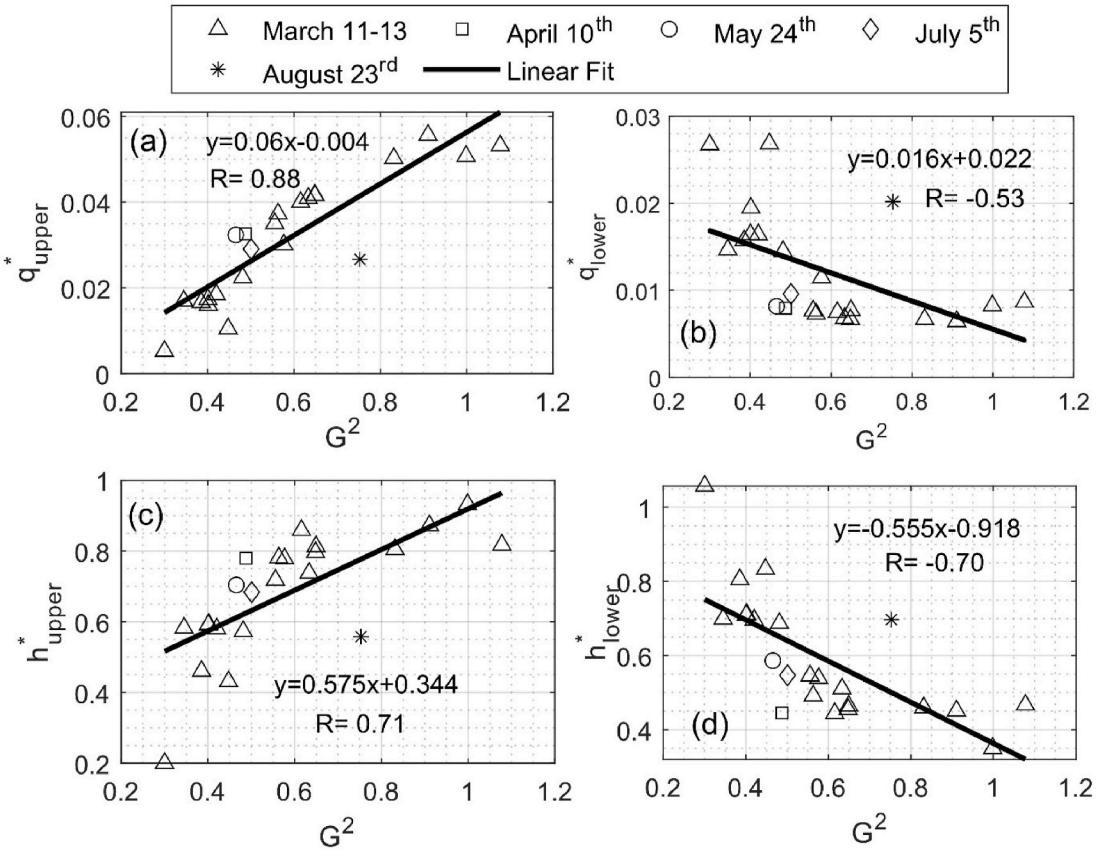


Fig. 16. The relation between Composite Froude number (G^2) and non-dimensional layer properties (layer volume fluxes and thicknesses).

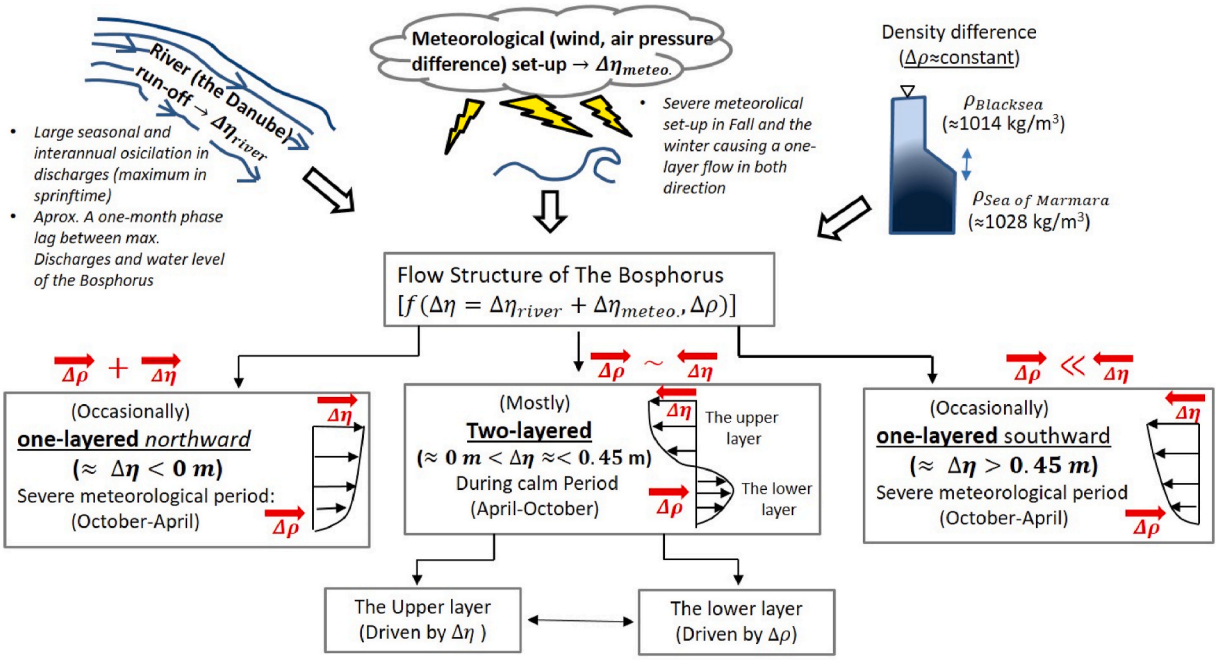


Fig. 17. The sketch diagram of the main findings of the present study.

structure (Fig. 9a-b-c) of the strait for around 45 days from late spring to early summer. This period of the year and the rest of the summer is meteorologically calm (Fig. 4a and c) and, as a result, the water level difference is much more stable during this time as compared to the rest of the year (Fig. 5a).

- Both the current observations at the closely located points (St. A, St. B, and St. C in Fig. 2) and at the cross-sectional line show that topography (i.e., a bottom sill or alteration in the course of the waterway) play decisive qualitative and quantitative roles in the local current structure (Fig. 9a-b-c, 11c, 12, and 13). The results also

demonstrate that flow velocities show significant variations in behavior between the main channel and the slopes of the cross-section. Taking profile measurements around the main channel point would be the most proper location to quantify stratification in a given waterway.

- The seasonal salinity and temperature variations are higher at the surface (Fig. 6a) than at the bottom (Fig. 6b). The notable fluctuations occurred in salinity (>5 PSU) and temperatures (~5 °C) in a short-term period (from a few days to a week) due to severe meteorological conditions that are evident during the fall and winter (Fig. 5a-b-c and 6a).
- The thickness of both layers and the mixed layer show significant variations in the strait (Figs. 7 and 8). In general, the stratification is stronger at both entrances (stronger at the Black Sea entrance) compared to the inner Bosphorus Strait, while the mixing is opposite in behavior.
- The salinity of both layers shows temporal variation both over depth and throughout the strait due to the strong mixing between layers. The salinity of the top layer is around 17 at the Black Sea entrance of the strait (Figs. 7 and 8). This value increases to 22 at the Sea of Marmara entrance. The salinities of the bottom layer are 38 at the south entrance and 32 to 35 at the north one.
- For $\Delta\eta \leq 0$ m and $\Delta\eta \geq 0.45$ m water level difference conditions, one layer flow dominates the whole cross-section in the southern part of the strait (Fig. 15a and c). For the remaining $\Delta\eta$s, however, the typical two-layer flow is observed. The correlations between the water level difference of the strait and the layer flow rates are notably higher at the upper layer ($R = 0.98$) than at the lower layer ($R = -0.90$), as $\Delta\eta$ is the driving force to the upper layer flow.
- The Bosphorus Strait has three control sections (the two sills at the south and the north, and the narrowest section in Fig. 1), where the maximal exchanges occur. The cross-sectional current measurements in the present study were performed on the line close to the southern sill (Figs. 1 and 2). The flow is mostly subcritical (Fig. 16a-b-c-d) except for some supercritical cases corresponding to a $\Delta\eta > 0.40$ m water level difference between both entrances of the strait.
- The relations between densimetric Froude number (G^2) and non-dimensional flow rates were also described to increase the applicability of the results to similar waterways. The maximum exchange ($q^*_{total} = q^*_{upper} + q^*_{lower}$) occurred $G^2 \approx 1$ (Fig. 16a and b) as two-layer flow hydraulics suggested. The corresponding non-dimensional flow rate and water depth were calculated as $q^*_{total} \cong 0.06$ and $h^*_{total} \cong 0.06$, respectively. The prediction capacity of the equations was higher for the upper layer one ($q^*_{upper} = 0.06 \times G^2 - 0.004,\ R = 0.88$) than for the lower layer one ($q^*_{lower} = 0.016 \times G^2 - 0.022,\ R = -0.53$).

CRediT authorship contribution statement

Mehmet Ozturk: Conceptualization, Investigation, Formal analysis, Writing – review & editing, Writing – original draft, Supervision, Methodology. **Furkan Altas:** Investigation.

Declaration of competing interest

The authors declare that they have no known competing financial interests or personal relationships that could have appeared to influence the work reported in this paper.

Acknowledgments

The authors wish to express their sincere thanks to the General Directorate of Marmaray Project of Ministry of Transportation, General Directorate of Ports, Airports and Railways Construction of Turkey, to let the evaluation of measured data in the Istanbul Bosphorus Strait. The efforts of TAISEI Corporation for the difficult measurement program and the efforts by AVRASYA Consultants are also acknowledged. We also wish to express our sincere thanks to Dr.Paul. A. WORK, Dr. Cihan Şahin and the Editor Dr. Steve Mitchell for their critics and contributions to improving the quality of the paper.

References

Alpar, B., Yuce, H., 1998. Sea-level variations and their interactions between the Black Sea and the Aegean Sea. Estuar. Coast Shelf Sci. 46, 609–619. https://doi.org/10.1006/ecss.1997.0285.

Altiok, H., Kayişoğlu, M., 2015. Seasonal and interannual variability of water exchange in the Strait of Istanbul. Mediterr. Mar. Sci. 16, 644–655. https://doi.org/10.12681/mms.1225.

Armi, L., Farmer, D.M., 1985. The internal hydraulics of the strait of Gibraltar and associated sills and narrows. Oceanol. Acta 8, 37–46.

Armi, L., 1986. The hydraulics of two layers with different densities. J. Fluid Mech. 163, 27–58.

Armi, L., Farmer, D.M., 1986. Maximal two-layer exchange through a contraction with barotropic net flow. J. Fluid Mech. 164, 27–51.

Armi, L., Farmer, D.M., 1988. The flow of Atlantic water through the Strait of Gibraltar. Prog. Oceanogr. 21 (1), 1–105. https://doi.org/10.1016/0079-6611(88)90055-9.

Besiktepe, S.T., Ozsoy, E., Unluata, U., 1993. Filling of the Marmara Sea by the Dardanelles lower layer inflow. Deep-Sea Res. Part I 40 (9), 1815–1838.

Blain, C.A., Cambazoglu, M.K., Kourafalou, V.H., 2009. Modeling the Dardanelles Strait outflow plume using a coupled model system. In: Oceans 2009 MTS/IEEE Biloxi Conference, 26-29 Oct. 2009, Biloxi, MS, USA.

Bruno, M., Chioua, J., Romero, J., Vázquez, A., Macías, D., Dastis, C., Ramírez-Romero, E., Echevarria, F., Reyes, J., García, C.M., 2013. The importance of sub-mesoscale processes for the exchange of properties through the Strait of Gibraltar. Prog. Oceanogr. 116, 66–79. https://doi.org/10.1016/j.pocean.2013.06.006.

Candela, J., Winant, C.D., Bryden, H.L., 1989. Meteorologically forced subinertial flows through the strait of Gibraltar. J. Geophys. Res. 94 (C9), 12,667–12,679. https://doi.org/10.1016/j.dsr.2008.05.008.

Çeçen, K., Bayazıt, M., Sümer, M., Güçlüer, S., Doğusal, M., Yüce, H., 1981. İstanbul Boğazı'nın Hidrolik Ve Oşinografik Etüdü (The Hydraulic and Oceanographic Survey of Istanbul Strait). Istanbul Technical University, Istanbul, Turkey.

Çolpan Polat, S., Tugrul, S., 1995. Nutrient and organic carbon exchanges between the Black and Marmara seas through the Bosphorus Strait. Continent. Shelf Res. 15, 1115–1132. https://doi.org/10.1016/0278-4343(94)00064-T.

Deniz, A., Özdemir, E.T., Sezen, İ., Coşkun, M., 2013. Investigations of storms in the region of Marmara in Turkey. Theor. Appl. Climatol. 112, 61–71. https://doi.org/10.1007/s00704-012-0715-x.

Doğan, E., Sur, H.İ., Sarıkaya, H.Z., Öztürk, İ., Güven, K.C., Kunter, A., Yüce, H., Okuş, E., Alpar, B., 2001a. Water Quality Monitoring, Third Progress Report, January General Directorate of Istanbul Water and Sewerage Administration. (ISKI) and Istanbul University Institute of Marine Sciences and Management.

Doğan, E., Sur, H.İ., Güven, K.C., Okuş, E., Balkis, N., Kiratli, N., Yüksek, A., Uysal, A., Ünlü, S., Altıok, H., Gazioğlu, C., Taş, S., Aslan, A., Yilmaz, N., Müftüoğlu, A.E., Cebeci, M., 2001b. Water Quality Monitoring, Final Report (2000). General Directorate of Istanbul Water and Sewerage Administration (ISKI) and Istanbul University Institute of Marine Sciences and Management.

Farmer, D.M., Armi, L., 1988. The flow of Mediterranean Water through the strait of Gibraltar. Prog. Oceanogr. 21 (1), 1–105. https://doi.org/10.1016/0079-6611(88)90055-9.

Global Runoff Data Centre (GRDC), 2007. Federal Institute of Hydrology, Germany. http://grdc.bafg.deS.

Gregg, M.C., Özsoy, E., 2002. Flow, water mass changes, and hydraulics in the Bosphorus. J. Geophys. Res. 107 https://doi.org/10.1029/2000JC000485.

Gunduz, M., Ozsoy, E., 2016. On Water Transport Variability of the Bosphorus Strait. The Sea of Marmara Marine Biodiversity, Fisheries, Conservation and Governance. Turkish Marine Research Foundation, pp. 118–134. Publication No:42.

Güler, I., Yüksel, Y., Yalçiner, A.C., Çevik, E., Ingerslev, C., 2006. Measurement and evaluation of the hydrodynamics and secondary currents in and near a strait connecting large water bodies-A field study. Ocean. Eng. 33, 1718–1748. https://doi.org/10.1016/j.oceaneng.2005.10.016.

Harzallah, A., 2008. Flow variability in the Strait of Gibraltar: the Mediterranean adjustment to tidal forcing. Deep-Sea Res. I 56, 459–470. https://doi.org/10.1016/j.dsr.2008.12.001.

Hubareva, E., Svetlichny, L., Kideys, A., Isinibilir, M., 2008. Fate of the Black Sea Acartia clausi and Acartia tonsa (Copepoda) penetrating into the Marmara Sea through the Bosphorus. Estuar. Coast Shelf Sci. 76, 131–140. https://doi.org/10.1016/j.ecss.2007.06.009.

Jarosz, E., Teague, W.J., Book, J.W., Beşiktepe, Ş., 2011. Observed volume fluxes in the Bosphorus Strait. Geophys. Res. Lett. 38 https://doi.org/10.1029/2011GL049557.

Kanarska, Y., Maderich, V., 2008. Modeling of seasonal exchange flows through the Dardanelles Strait. Estuarine. Coastal Shelf Sci. 79, 449–458. https://doi.org/10.1016/j.ecss.2008.04.019.

Koşucu, M.M., Demirel, M.C., Kırca, V.S.O., Özger, M., 2019. Hydrodynamic and hydrographic modeling of Istanbul strait. Processes 7 (10), 710. https://doi.org/10.3390/pr7100710.

Lacombe, H., Richez, C., 1984. Hydrology and Currents in the Strait of Gibraltar. Office of Naval Research, NORDA. Sea Straits Report 3.

Latif, M.A., Özsoy, E., Oguz, T., Ünlüata, Ü., 1991. Observations of the Mediterranean inflow into the Black Sea. Deep-Sea Res. Part A Oceanogr. Res. Pap. 38, S711–S723. https://doi.org/10.1016/S0198-0149(10)80005-6.

Maderich, V., Konstantinov, S., 2002. Seasonal dynamics of the system sea-strait: Black Sea–Bosphorus case study. Estuar. Coast Shelf Sci. 55 (2), 183–196. https://doi.org/10.1006/ecss.2001.0895.

Maderich, V., Ilyin, Y., Lemeshko, E., 2015. Seasonal and interannual variability of the water exchange in the Turkish Straits System estimated by modelling. Mediterr. Mar. Sci. 16 (2), 444–459. https://doi.org/10.12681/mms.1103.

Murray, S., Johns, W., 1997. Direct observations of seasonal exchange through the Bab el Mandab Strait. Geophys. Res. Lett. 24, 2557–2560. https://doi.org/10.1029/97GL02741.

Oguz, T., Özsoy, E., Latif, M.A., Sur, H.I., 1990. Ünlüata, Ü. Modeling of hydraulically controlled exchange flow in the Bosphorus Strait. J. Phys. Oceanogr. 20, 945–965.

Oguz, T., 2005. Hydraulic adjustments of the Bosphorus exchange flow. Geophys. Res. Lett. 32 (6) https://doi.org/10.1007/s10236-016-1026-z.

Ottesen Hansen, N., Møller, J., 1990. Zero blocking solution for the Great Belt link. In: Pratt, L. (Ed.), The Physical Oceanography of Sea Straits. Kluwer, pp. 153–170. https://doi.org/10.1007/978-94-009-0677-8_6.

Ozturk, M., Sahin, C., Yuksel, Y., 2017. Current power potential of a sea strait: the Bosphorus. Renew. Energy 114 (Part A), 191–203. https://doi.org/10.1016/j.renene.2017.04.003, 2017.

Özdemir, E.T., 2018. Mega Şehir İstanbul'un Fırtınalarının Araştırılması (Investigation of storms of mega city Istanbul). Selcuk Univ. J. Eng. Sci. Technol. 6 (2), 331–342. https://doi.org/10.15317/Scitech.2018.136. In Turkish.

Özsoy, E., Latif, M.A., Sur, H.I., Goryachkin, Y., 1996. A review of the exchange flow regime and mixing in the Bosphorus Strait. Bulletin de l'Institut Oceanographique de Monaco 2, 187–204.

Özsoy, E., Beşiktepe, Ş., Latif, M.A., 2000. Türk Boğazlar Sistemi'nin Oşinografisi (Oceanography of the Turkish strait system). In: Marmara Denizi 2000 Sempozyumu; Türk Deniz Araştırmaları Vakfı: Istanbul, Turkey.

Özsoy, E., Cagatay, M.N., Balkis, N., Balkis, N., Ozturk, B., 2016. The Sea of Marmara; Marine Biodiversity, Fisheries, Conservation and Governance. Turkish Marine Research Foundation (TUDAV) Publication, Istanbul, Turkey, ISBN 9789758825349.

Öztürk, M., Ayat, B., Aydoğan, B., Yüksel, Y., 2012. 3D numerical modeling of stratified flows: case study of the Bosphorus Strait. Journal of Waterway Port Coastal Ocean Eng.ASCE 138, 406–419. https://doi.org/10.1061/(asce)ww.1943-5460.0000132.

Öztürk, M., 2013. Numerical modeling of effect of duration of barotropic forcing on sea strait flow: case study of the Bosphorus Strait. ASCE J. Hydraulic Eng. 139 (11), 1199–1211. https://doi.org/10.1061/(ASCE)HY.1943-7900.0000783.

Sumer, B.M., Bakioglu, M., 1981. Sea-Strait Flow with Special Reference to Bosphorus. Technical Report. IstanbulTechnical University-Civil Engineering Faculty, Istanbul, Turkey.

Stanev, V.E., Peneva, E., 2002. Regional sea-level response to global climatic change: Black Sea examples. Global Planet. Change 32, 33–47. https://doi.org/10.1016/S0921-8181(01)00148-5.

Sur, H.I., Özsoy, E., Ünlüata, Ü., 1994. Boundary current instabilities, upwelling, shelf mixing and eutrophication processes in the Black Sea. Prog. Oceanogr. 33, 249–302. https://doi.org/10.1016/0079-6611(94)90020-5.

Ünlüata, Ü., Oğuz, T., Latif, M.A., Özsoy, E., 1990. On the physical Oceanography of Turkish straits. In: Pratt, L.J. (Ed.), The Physical Oceanography of Sea Straits. Kluwer, Dordrecht, pp. 25–60. NATO/ASI Series.

Yazicioglu, H., Tunc, K.M.M., Ozbek, M., Kara, T., 2016. Simulation of electricity generation by marine current turbines at Istanbul Bosphorus Strait. Energy 95 (C), 41–50. https://doi.org/10.1016/j.energy.2015.11.038.

Yuksel, Y., Ayat, B., Ozturk, M.N., Aydogan, B., Guler, I., Ozkan Cevik, E., Yalçıner, A.C., 2008. Responses of the stratified flows to their driving conditions a field study. Ocean. Eng. 35, 1304–1321. https://doi.org/10.1016/j.oceaneng.2008.06.006.